HHS Public Access

Author manuscript

J Mol Cell Cardiol. Author manuscript; available in PMC 2020 February 01.

Published in final edited form as:

J Mol Cell Cardiol. 2019 February ; 127: 97–104. doi:10.1016/j.yjmcc.2018.11.021.

Real-time local oxygen measurements for high resolution cellular imaging

Liron Boyman[a,b,*], **George S. B. Williams**[a,b,*], **Andrew P. Wescott**[a,b], **Jennie B. Leach**[c], **Joseph P. Y. Kao**[a,b], and **W. Jonathan Lederer**[a,b]

[a]Center for Biomedical Engineering and Technology, University of Maryland School of Medicine, Baltimore, Maryland 21201 USA

[b]Department of Physiology, University of Maryland School of Medicine, Baltimore, Maryland 21201 USA

[c]Department of Chemical, Biochemical and Environmental Engineering, University of Maryland Baltimore County, Baltimore MD 21250

Abstract

Single-cell metabolic investigations are hampered by the absence of flexible tools to measure local partial pressure of O_2 (pO_2) at high spatial-temporal resolution. To this end, we developed an optical sensor capable of measuring local pericellular pO_2 for subcellular resolution measurements with confocal imaging while simultaneously carrying out electrophysiological and/or chemo-mechanical single cell experiments. Here we present the OxySplot optrode, a ratiometric fluorescent O_2-micro-sensor created by adsorbing O_2-sensitive and O_2-insensitive fluorophores onto micro-particles of silica. To protect the OxySplot optrode from the components and reactants of liquid environment without compromising access to O_2, the microparticles are coated with an optically clear silicone polymer (PDMS, polydimethylsiloxane). The PDMS coated OxySplot micro-particles are used alone or in a thin (~50 micron) PDMS layer of arbitrary shape referred to as the OxyMat. Additional top coatings on the OxyMat (e.g., fibronectin, laminin, polylysine, special photoactivatable surfaces etc.) facilitate adherence of cells. The OxySplots report the cellular pO_2 and micro-gradients of pO_2 without disrupting the flow of extracellular solutions or interfering with patch-clamp pipettes, mechanical attachments, and micro-superfusion. Since OxySplots and a cell can be imaged and spatially resolved, calibrated changes of pO_2 and intracellular events can be imaged simultaneously. In addition, the response-time ($t_{0.5}$ = 0.7 s, 0 - 160 mm Hg) of OxySplots is ~100 times faster than amperometric Clark-type polarization microelectrodes. Two usage example of OxySplots with cardiomyocytes show (1) OxySplots measuring pericellular pO_2 while tetramethylrhodamine methyl-ester (TMRM) was used to measure mitochondrial membrane potential ($\Delta\Psi_m$); and (2) OxySplots measuring pO_2 during ischemia and reperfusion while rhod-2 was used to measure cytosolic $[Ca^{2+}]_i$ levels

Corresponding Author: W. Jonathan Lederer, Center for Biomedical Engineering and Technology, University of Maryland School of Medicine, Baltimore, Maryland 21201 USA, Tel: 410-706-4895, FAX: 410-510-1545, jlederer@som.umaryland.edu.

*Contributed equally to this work

simultaneously. The OxySplot/OxyMat optrode system provides an affordable and highly adaptable optical sensor system for monitoring pO_2 with a diverse array of imaging systems, including high-speed, high-resolution confocal microscopes while physiological features are measured simultaneously.

Keywords

Calcium; Mitochondria; Mitochondrial Calcium Uptake; Mitochondrial Calcium Uniporter; Calcium signaling in heart; oxygen optrode

1. Introduction

Under normal physiological conditions, the mitochondrial electron transport chain consumes cellular oxygen (O_2) to generate a proton motive force, which powers ATP synthesis by complex V, the ATP synthase. Thus, many cellular processes that depend on [ATP] are either directly or indirectly regulated by the availability of O_2 to the cells. Restriction of tissue blood flow reduces the O_2 supply and produces tissue ischemia which, when prolonged, is detrimental to virtually all cell types. The time and spatial details of the O_2 deprivation associated with ischemia matter. Thus, to investigate how ischemia causes cellular damage it is important to obtain rapid, accurate, and reliable measurements as the O_2 level declines, remains low, and rises again. For example, although restoration of blood flow can fix an ischemic event, it can also have adverse effects. Cell damage or death may occur as a result of the reperfusion due to “Ischemia-Reperfusion” (IR) injury [1–5]. The extent of IR damage may depend on the time and degree of O_2 deprivation and the circumstances surrounding the reperfusion. In the intact heart, IR injury that follows acute myocardial infarction, for example, can cause massive loss of cardiomyocytes. Since cardiomyocytes as a rule do not regenerate following cell death, IR cell damage or loss may underlie contractile dysfunction and/or lethal arrhythmia[1, 6]. Yet, despite decades of study and the severity of IR damage, it is not clear what the primary processes that develop during the ischemic phase are, and it is also unclear how this damage predisposes the myocytes to abrupt cell death on reperfusion. The tools described here enable one to control and measure the partial pressure of O_2 (pO_2) in experiments carried out in single cells or small clusters of myocytes -- while other cellular features are measured simultaneously. This method thus enables one to accurately investigate the details of the cellular changes associated with ischemia and also the details of cellular pathology produced by IR injury. These same tools could be used by others to study nearly any cell type and how O_2 affects them quantitatively.

The core method widely used in biology to measure O_2 is the Clark-type electrode, a polarization electrode, the output of which is proportional to pO_2 [7–9]. The technology is robust and widely used. There are two primary problems for single cell experiments: (1) the large size and (2) the slow response of the Clark-type electrodes. More recently custom fabrication of miniaturized Clark-type electrode system was described [10] and additional industrial and scientific sensors have been developed. This includes the solid-state zirconium dioxide O_2 sensor [11], or a proprietary fiber optic method by Ocean Optics that has improved response time and diverse uses [12]. However, such sensors require dedicated

instrumentation, custom fabrication, and an associated electronics package. Other optical sensors, such as MitoXpress, do not require such specialized instrumentation. These are phosphorescent O_2 sensors that can be simply added to the extracellular superfusion solution for liposomal cellular uptake or coupled to a biopolymer carrier that can be endocytosed [13]. To photo-stabilize the phosphorescent molecules in the intracellular environment further improvement of these sensors included imbedding the sensors into nano-beads[14]. However, the cytotoxicity [15, 16] of the nano-beads via unclear mechanisms and other practical drawbacks such as the need to load the beads by permeabilization and the partial intracellular dispersion have limited the extent to which this approach is applied. Here, we describe a non-invasive method for measurements of O_2 in experiments with single cells that is ideally suited for virtually any adherent cell type. We make use of Ruthenium based fluorescent optical sensors, which were originally developed for large scale process control [17–20]. With miniaturization, these sensors form the basis of the system presented here and those marketed by others in proprietary formulations. They are robust fluorescent sensors for O_2 and have been used widely in other applications[20, 21]. Agilent/Seahorse uses a proprietary micro well plate technology with this indicator for metabolic investigations of populations of cells or isolated mitochondria in a micro-well configuration[22]. Here, we describe a ruthenium/nile blue based ratiometric method that has been miniaturized for use with isolated single cells being imaged on a microscope. While readily used with glass coverslips and other microscopy tools, it is also adaptable by the imaginative scientist. Briefly, OxySplots is the name given to the new optical tool described here that permits rapid oxygen measurements of pO_2. We provide information needed to make and use OxySplots. It consists of silicone coated micron sized silica gel powder to which two fluorescent chemicals have been adsorbed: (1) the O_2-sensitive $Ru(Ph_2phen_3)Cl_2$ and (2) the O_2-insensitive Nile blue chloride. Thin (~50 microns) clear PDMS coating containing OxySplots polymerizes on a #1 glass coverslip. The cells placed above the PDMS are imaged as are the OxySplots. This approach allows for the measurement of the partial pressure of O_2 (pO_2) over the range of 0 – 160 mmHg in the cell's local microenvironment (i.e., pericellular region). The measurements of pO_2 are carried out along with critical intracellular processes (e.g., $[Ca^{2+}]_i$ transients, mitochondrial membrane potential ($\Delta\Psi_m$), etc.) at fast rates and high spatial resolution.

2. Methods

A detailed description of OxySplots preparation and other materials and methods used here can be found in the expanded Online Data Supplement. Briefly, imaging was done with Nikon A1R inverted confocal microscope (Nikon, Japan) and with a Zeiss LSM 510 inverted confocal microscope (Carl Zeiss, Jena, Germany). Ventricular myocytes were isolated using standard enzymatic approaches [23] from rats or rabbits. $\Delta\Psi_m$ was measured by supplementing the extracellular bathing solution with 30 nM of TMRM (Tetramethylrhodamine Methyl Ester Perchlorate). $[Ca^{2+}]_i$ transients were measured in cardiomyocytes using the acetoxymethyl (AM) ester form of the Ca^{2+} indicator Rhod-2 (Rhod-2 AM) to load the cells with Rhod-2, and were acquired using the confocal line-scan mode. All experiments were conducted at room temperature.

3. Results

A method is presented and demonstrated that enables high-resolution single cell experiments to be carried out while simultaneously measuring the partial pressure of O_2 (pO_2) locally at high speed. We are able to do this by coating the removable bath bottom (a 25 mm #1 glass coverslip) with a thin layer (~50 micron) of oxygen-permeable PDMS (polydimethylsiloxane) into which we have embedded OxySplots (See Fig. 1A). After applying an optional coating to the PDMS (e.g. fibronectin, polylysine, etc.), the freshly isolated cells (cardiac ventricular myocytes in the examples shown here) are added in a physiological solution to the bath and allowed to settle (See Fig. 1B). We can then carry out our experiments. For some experiments, rods are attached to the non-adherent cells for chemo-mechanical experiments and they are lifted several microns from the PDMS surface; for other experiments the cell are allowed to attach to the PDMS or its coating. We can thus carry out a multitude of distinct and separate experiments with the OxySplots under the cells being investigated. The reporting on local pO_2 is from only tens of microns away from the cells and thus exquisitely relevant to the cells (See Fig. 1B). In addition to a gas-tight global bath superfusion source that can be switched between tunable pO_2 sources, a gas-tight glass microperfusion system is available to delivery local solution if needed with variable pO_2 to a specific cell under study. This combination of definable pO_2 sources enables pO_2 to be changed quickly as demanded by the planned experiments and measured in real time by the OxySplots. The plume from the microperfusion can be adjusted to partially or fully cover the cell under investigation and the PDMS and the nearby OxySplots.

This system enables one to carry out physiological experiments on single cells with a defined level of pO_2 and to change the pO_2 level as required by the experiments. The method thus allows one to measure pO_2 within the microenvironment of isolated or adherent cells (e.g., cardiomyocytes, smooth muscle, model cells, and small tissue components) and investigate how pO_2 may affect cell function and other variables. Since the system is designed to work on confocal, multiphoton, structured illumination, widefield or super-resolution microscopes, the cell biology, physiology and pathophysiology of these cells can be studied simultaneously.

3.1. Calibration of the OxySplots.

To provide quantitative pO_2 measurements, we first carried out a calibration of the OxySplots using a traditional O_2-microelectrode as a pO_2 reference. The tip of the O_2 microelectrode is bathed in the chamber's solution (total bath volume 250–300 μL), and positioned approximately 50 pm above the confocal imaging plane of the silica gel microparticles. To rapidly equilibrate the O_2-microelectrode and the fluorescent O_2-probe with a set level of pO_2, the flow-rate of the gassed solution into the chamber is 20 mL min"[1]. The solution reservoir is bubbled with argon and with air. The flow ratio of the two gasses made it possible to vary the bath pO_2 in controlled increments.

Because the OxySplots are plentiful and randomly distributed each OxySplots is identified by binary image conversion (see Supplemental Fig. 2D) with respect to its location. The fluorescence signal of each OxySplots and how it changes over time is then obtained from the time-lapse confocal images of multiple OxySplots. Note, this was performed using the

particle identifier plug-in from the ImageJ software. The fluorescence signals obtained from the OxySplots during the calibration procedure are shown in the inset of Supplemental Fig. 1. From this, a time-dependent fluorescence ratio (R) is measured from each OxySplot. The ratio consists of the signal from the O_2-sensitive fluorophore $Ru(Ph_2phen_3)Cl_2$ divided by the O_2-insensitive fluorophore Nile blue chloride and allows for correction of non-oxygen related changes (e.g., movement artifacts). Figure 2A shows the pO_2 measurements with the fluorescent O_2-probe (n=107 particles), and the simultaneous pO_2 reading from the O_2-microelectrode. To facilitate the comparison, the measurements are normalized to ambient room conditions (i.e., pO_2 = 160 mmHg, R_{160}). Note that the fluorescence emission intensity of an immobilized transition metal-complex, such as $Ru(Ph_2phen_3)Cl_2$, becomes quenched due to O_2 binding to $Ru(Ph_2phen_3)Cl_2$ (see Supplemental Fig. 1. and Supplemental Movie 2). The dependency of the fluorescence ratio for the OxySplots (R) on pO_2 can therefore be described by a 2-site Stern-Volmer model[24],

$$\frac{R}{R_{160}} = \frac{\left(\frac{R_0}{R_{160}}\right)\left(K_{sv}\left(pO_2 - f_1\, pO_2\right) + 1\right)}{K_{sv} pO_2 + 1} \quad (1)$$

where R_0 is the fluorescence ratio at 0 mmHg, f_1 is the fraction of the immobilized $Ru(Ph_2phen_3)Cl_2$ population that can become quenched, and K_{sv} is the Stern-Volmer quenching constant. Our tests (see Fig. 2) suggest that under these conditions the large majority of the $Ru(Ph_2phen_3)Cl_2$ molecules can become quenched by O_2 (f_1=0.96 ± 0.02). Other constants (R_0 / R_{160}=2.85 ± 0.06, K_{sv}= 0.012 ± 0.001 $mmHg^{-1}$) have comparable values to those reported by others [19, 24]. Having determined these parameters, fluorescence measurements of pO_2 can now be quantified using ambient room conditions (i.e., R_{160}) as a null-point (see Supplemental Table 1) by rearranging equation 1 to give,

$$pO_2 = \frac{\left(R_A - R_B\right)}{K_{sv}\left(R_B + R_A(f1 - 1)\right)} \quad (2)$$

where $R_A = R_0/R_{160}$ and $R_B=R/R_{160}$. Note, R_A is determined by the calibration shown in Fig. 2 and can be assumed to be a constant over the lifespan of the OxySplots. In addition, the inherent steady-state quenching constants of $Ru(Ph_2phen_3)Cl_2$ (i.e., f_1 and K_{sv}) are not expected to vary in bathing solutions of different compositions because the polydimethylsiloxane (PDMS) gel is gas-permeable but it is impermeable to ions. Note also that the diffusion rate of O_2 through PDMS is roughly the same as though H_2O (2.4×10^{-5} cm^2/s at 25° C, see Supplemental Table 2), which makes PDMS an ideal encapsulating material for measuring local, pericellular pO_2. On the other hand, it is critical that other materials which deliver or retain the perfusion solutions be significantly less permeable to O_2 (see Supplemental Table 2) as atmospheric oxygen at ambient room conditions can rapidly contaminate hypoxic solutions. Importantly, even if anoxic solutions flow rapidly and travel relatively short distances through plastic tubing (or even metal), by the time they reach the cellular imaging chamber they are contaminated with O_2 (see Supplemental Fig.

2). This highlights the importance of continually monitoring pericellular pO_2 using a technique such as the one we present here when conducting experiments that require controlled hypoxia.

3.2. Testing the spatiotemporal resolution of the OxySplots.

One significant advantage of the OxySplots over traditional approaches is the ability to carry out spatially resolved measurements of pO_2. To mimic a localized O_2 contamination we perfused solution contaminated by O_2 via a micro-perfusion manifold into a bath bulk perfused with an anoxic solution. The OxySplots enable this contamination to be visualized with high spatial resolution (see Fig. 3A). While the contaminated region is relatively small (i.e., < 0.5 mm^2), this area could easily encompass multiple cells and might go unnoticed using existing pO_2 measurement techniques (e.g., micro-electrode). Furthermore, because the OxySplots are plentiful their individual measures of pO_2 can be combined via 2D interpolation into a “heatmap” of pO_2 surround the cells (see Fig. 3B) enabling the OxySplots to provide unprecedented details regarding the microenvironment of a cell.

To estimate the response-time of the OxySplots to abrupt changes of pO_2, a local microperfusion system was devised. The OxySplots are first perfused with anoxic bathing solution then a hyperoxic solution is applied via the microperfusion system (see Fig. 3A). By adding an O_2-insensitive fluorophore, sulforhodamine, to the hyperoxic solution we can monitor the light absorption by sulforhodamine as confirmation of bathing solution exchange (see Supplemental Fig. 3). Abrupt step changes of pO_2 lead to reciprocal and rapid changes in $Ru(Ph_2phen_3)Cl_2$ fluorescence (see Fig. 3A). Our tests indicate that the fluorescent O_2-probe can capture an 80 mmHg pO_2 rise within 0.7 seconds, and a decay of identical magnitude within 1.63 seconds (see Fig. 4C). This confirms that our fluorescent O_2-probe is capable of accurately and rapidly reporting changes in pO_2.

3.3. Parallel measurements of pericellular pO_2 and mitochondrial membrane potential ($\Delta\Psi_m$) of single cardiomyocytes.

Here we take advantage of this new approach to perform cellular time-lapse experiments with high spatial resolution. Since OxySplots are approximately 10-20 μm beneath the adherent cell, each can be resolved separately. This allows high spatial resolution confocal images to be captured from either the OxySplot (Fig. 5A) or cellular focal plane (Fig 5B). In these experiments cardiomyocytes are loaded with tetramethylrhodamine methyl ester (TMRM), which preferentially accumulate in the matrix of polarized (i.e., respiring) mitochondria. Since TMRM accumulation is directly proportional to the voltage gradient across the mitochondrial inner membrane (i.e., $\Delta\Psi_m$), its fluorescence is used for dynamic measurements $\Delta\Psi_m$. Figure 5C shows the ability of OxySplots to report pericellular pO_2 while $\Delta\Psi_m$ is monitored during a brief period (400 seconds) of hypoxia (see black line in Fig. 5C). While this brief exposure to hypoxia did not produce any significant change in $\Delta\Psi_m$, TMRM is ideal for reporting rapid changes in $\Delta\Psi_m$ [25]. Additionally, the ability to simultaneously monitor pericellular pO_2 and mitochondrial dynamics such as $\Delta\Psi_m$ will be crucial to future investigations into the role of mitochondria in IR injury.

3.4. Measuring $[Ca^{2+}]_i$ from single cardiomyocytes during ischemia-reperfusion.

Now we can test the capability of this new approach to provide dynamic measurements of cellular processes at high temporal resolution from single cells, and how they change during ischemia. To monitor rapid changes in cellular $[Ca^{2+}]$ ($[Ca^{2+}]_i$) and pericellular pO_2 the confocal microscope is programmed to quickly alternate between the focal planes of the OxySplots and the cardiomyocyte (see Fig. 6A). Here $[Ca^{2+}]_i$ is measured using the Ca^{2+}-sensitive fluorescent indicator Rhod-2. Throughout the experiment shown in Fig. 6A an isolated cardiomyocyte is electrically paced at 0.5 Hz via electrical field stimulation. Initially, under normal conditions (i.e., cell bathed with normal Tyrode's solution (NT) equilibrated with room air), a $[Ca^{2+}]_i$ transient and the corresponding cell contraction it induces can be observed following each field stimulus. Following the transition to the ischemic conditions (i.e., cell bathed with ischemic Tyrode's solution (IT)) pericellular pO_2 declines, and pronounced alterations in $[Ca^{2+}]_i$ are observed (see Fig. 6A-also see SD Fig 5). Note that the $[Ca^{2+}]_i$ transients quickly stabilize and remain in sync with the pacing rate during the 15 minutes of ischemic conditions. However, when the ischemic, extracellular solution is replaced with NT (i.e., reperfusion), asynchronous, oscillatory $[Ca^{2+}]_i$ signals occurred. Confocal images capture the cellular alterations can be captured as they occur (see Fig. 6Bi) and the final states of hypercontracture and cell necrosis (see Fig. 6Bii). By capturing pericellular pO_2 alongside critical cellular signaling processes the O_2 monitoring technique shown here allows for the careful consideration of O_2 as a key determinant in cell injury during pathophysiology.

4. Discussion

A new and extremely practical method is presented that enables any investigator to develop a simple, affordable, effective and rapid method to measure pO_2 on virtually any fluorescence microscope system. We have outlined our system and demonstrated its use in heart muscle cells. It can be customized for special needs and adapted to overcome unanticipated problems for virtually all cell types. The basic design of the pO_2 optrode probe is a nano-porous inert scaffold of silica gel (porous silicon dioxide) to which two fluorophores are adhered. One is quenched by O_2 ($Ru(Ph_2phen_3)Cl_2$) while the other (Nile blue chloride) is unaffected. The probes and scaffold structures are protected with the O_2-permeable PDMS and as functional units have been called OxySplots. As shown here the ratios of these signals can be quickly calibrated via a null-point formula (see below) so that the OxySplots accurately report pO_2 over the range of 0–160 mm Hg. Diverse experiments can be carried out when the OxySplots are incorporated in a thin layer of PDMS but for other experiments the OxySplots can be positioned in the same plane as the cells under investigation.

4.1. Null-point.

A new and simplified calibration procedure for OxySplots is also presented here allowing ambient room conditions (i.e., pO_2 = 160 mmHg, R_{160}) to serve as a null-point calibration thereby avoiding repeated calibrations of the same probe. This null-point correction eliminates the effects of possible instabilities in excitation/emission light intensities and also corrects the pO_2 measurements for possible gradual bleaching of the immobilized

fluorescent indicators. See “Calibration of the OxySplots” subsection located in the Results section above.

4.2. Ischemia.

The cellular, organellar, and molecular processes underlying ischemic cell injury remain poorly understood. It is clear however that many cell types -- even cardiomyocytes, which critically depend on continuous O_2 supply -- can adapt to episodes of reduces O_2 supply and ischemia. Irreversible cell injury (i.e., IR injury) does not necessarily occur after every ischemic episode. It has long been known from the work of Murry et al., 1986 [26] that cardiomyocytes have inherent adaptation mechanism(s) that, when triggered, can confer protection from subsequent ischemic episodes. Many critical questions remain regarding this discovery of ischemic adaptation, originally termed “ischemic-preconditioning”. Unfortunately, the available tools limit the ability to investigate this adaptation processes (as well as others) with high spatiotemporal resolution.

Techniques to measure pathological intracellular processes in real-time during ischemia have so far been primarily limited to the use of the halted-flow, whole-heart system. Many critical discoveries have been made possible through the frequent use of this system; however, its usage does entail several critical disadvantages. For example, inducing ischemia by halting the flow through major coronary arteries while the heart is exposed or fully exteriorized creates varying levels of ischemia through the myocardium. In addition, the signal measured in these systems is tissue level (i.e., multi-cellular) causing signals from near epicardial layers to comingle with those arising from deeper layers near the ischemic myocardial core.

Single-cell experiments such as those presented here allow the pericellular pO_2 to be tightly controlled thereby avoiding the tissue-level limitations described above. The types of single cell experiments presented here are timely, as is the ability to measure intracellular signals alongside pericellular pO_2. These data provide a direct means for the first time to link changes in pO_2 levels (surrounding the cell) with changes of critical intracellular variables. These challenges (and others) have inspired us to develop an O_2 monitoring system compatible with high resolution confocal measurements of critical cellular components (e.g., mitochondria) allowing rapid alterations and measurements of pericellular pO_2. Furthermore, the ability to resolve dynamic mitochondrial signals at high resolution with pericellular pO_2 is valuable for additional reasons. For example, explicit evidence reveals that mitochondria are damaged during cardiac IR [27] but the time-course and molecular details of this process remain elusive. It has been argued that a large conductance channel across the IMM opens during IR [28–39]. Our ability to observe and characterize this channel (the mitochondrial permeability transition pore, mPTP) during IR, will be significantly enhanced by the use of the technique presented here.

4.3. Contamination of hypoxic solutions by atmospheric O_2.

Here we also demonstrate how the OxySplots technique can provide new means to precisely control the pericellular pO_2. This is significant as single-cell experiments can be easily contaminated by atmospheric O_2. In fact, we found that even when our buffer reservoir was heavily bubbled with 100% Ar to completely remove the dissolved O_2 as measured by a

dipped Clark-type electrode, the measured pericellular perfusate pO_2 was significantly higher. This required additional modifications of the system. In addition, we confirmed that even when using materials with low O_2 permeability to carry hypoxic solutions, contamination is very likely. We quantified this behavior (see Supplemental Table 2) to aid future material selections. Furthermore, clearance of pericellular O_2 is not a rapid process, even when this is done with solutions saturated with a heavy inert gas such as argon, which yields a stagnant gaseous phase limiting reentry of O_2. Thus, the ability to measure pericellular pO_2 is critical so that induced ischemic and hypoxic conditions could be confirmed and carefully adjusted.

4.4. Other existing technologies for measurements of pO_2 in single cells experiments.

The acute need to understand better how the availability of O_2 is involved in physiological and pathophysiological mechanisms within cells has prompted the development of pO_2 measurement technologies, including the one presented here. The goal is the simultaneous measurement of pO_2 and other important signals from the single cells under study. However, the technologies available before OxySplots have generally been inconvenient and in some cases cumbersome. Polarization-electrodes like the classic Clark electrode [10] or fiber-optic electrodes [12] require specialized or customized fabricated instrumentation and may interfere with patch clamp hardware or micro-tools used in mechanotransduction experiments. Other intriguing technologies include “nanobead” pO_2 sensors. However, the use of nanobead phosphorescent O_2 sensors [14] has serious drawbacks. The phosphorescent molecules are embedded in the nanobeads composed of one of several plastics that must be microinjected, endocytosed or require prolonged (hours) liposomal loading or aggressive electroporation [14]. These phosphorescent nanobead sensors are not readily compatible with many isolated primary cells such as cardiomyocytes. In addition, the nanobeads may alter physiology or be cytotoxic [15, 16, 40].

4.5. Diverse potential applications.

While we present two applications for the use of OxySplots in single cell experiments, the potential uses are nearly unlimited. Beyond investigating cardiomyocytes, the layered application of OxySplots could be used to investigate nearly any adherent cell type (e.g., HeLa cells, neurons, HEK-293, etc.) using a confocal microscope. Even small organisms (e.g., C. elegans, yeast, bacteria, etc.) could be placed above the OxySplots layer. In addition to confocal measurements, the OxySplots could be arranged in small blobs (see Supplementary Data, Fig. 4, illustration) making the approach compatible with a diverse array of wide-field imaging techniques. In SD-Fig. 4, we show a schematic drawing where the cells and the OxySplots are in the same focal plane but they are laterally displaced. This arrangement enables the two signals to be spatially resolved within the same image and acquired at the same time. Additionally, if OxySplots were placed within a closed system that included an oxygen-consuming cell or organism, O_2 consumption could be measured. Such a enclosure would constitute a microscope-based respirometer. Clearly, there are many additional potential applications.

Oxysplots.—While OxySplots are unusually robust and adaptable sensors for the measurement of pO_2, they have limitations. While the adsorbed dyes on the micron-sized

silica gel powder last a very long time (years) when kept cool and dry, the PDMS embedded sensors (OxySplots) has a shelf life of about 6 months. See Supplementary Data for preparation of sensors and OxySplot details. Additionally, while outstanding in reporting pO_2 over the range of 0 mm Hg to 160 mm Hg as shown in Fig. 2, the OxySplots are less sensitive at higher O_2 levels.

4.6. Overview.

A versatile and inexpensive oxygen optrode has been developed for use with single cells, small tissue samples as well as cells in culture when examined with state-of-the-art fluorescence microscopes. The nickname for the optrode is OxySplot to reflect its rapid full-range sensitivity to oxygen, its amorphous and variable shape, and small size. Simple demonstration of its calibration and utility have been provided. With this technology, there is now no longer any need to simply or blindly "set" the pO_2 at its source level and assume that it will be delivered unchanged. Instead, now, the pO_2 can be readily measured at the cellular target while simultaneously measuring electrical, mechanical and physiological properties.

Supplementary Material

Refer to Web version on PubMed Central for supplementary material.

Acknowledgments

7. Funding

This work was supported by American Heart Association Grant 15SDG22100002 (LB), and 16PRE31030023 (to A.P.W.), and NIH grants; R01 HL106056 (WJL), R01 HL105239 (WJL), U01 HL116321 (WJL), F32 HL108604 (GSBW), and K25 HL125762 (GSBW).

Abbreviations

$[Ca^{2+}]_i$	cytosolic free calcium
$[Ca^{2+}]_m$	mitochondrial matrix free calcium
IMM	inner mitochondrial membrane
$\Delta\Psi_m$	the voltage gradient across the inner mitochondrial membrane
MCU	the mitochondrial Ca^{2+} uniporter
NCLX	the mitochondrial sodium calcium exchanger
jSR	the junctional sarcoplasmic reticulum
pO_2	partial pressure of O_2

10. References

[1]. Jennings RB, Historical perspective on the pathology of myocardial ischemia/reperfusion injury, Circ Res 113(4) (2013) 428–38. [PubMed: 23908330]

[2]. Dietrich WD, Morphological manifestations of reperfusion injury in brain, Ann N Y Acad Sci 723 (1994) 15–24. [PubMed: 8030862]

[3]. Blaisdell FW, The pathophysiology of skeletal muscle ischemia and the reperfusion syndrome: a review, Cardiovasc Surg 10(6) (2002) 620–30. [PubMed: 12453699]

[4]. Saidi RF, Kenari SK, Liver ischemia/reperfusion injury: an overview, J Invest Surg 27(6) (2014) 366–79. [PubMed: 25058854]

[5]. Murry CE, Jennings RB, Reimer KA, Preconditioning with ischemia: a delay of lethal cell injury in ischemic myocardium, Circ. 74 (1986) 1124–1136.

[6]. Hausenloy DJ, Yellon DM, Myocardial ischemia-reperfusion injury: a neglected therapeutic target, J Clin Invest 123(1) (2013) 92–100. [PubMed: 23281415]

[7]. Clark LC Jr., Wolf R, Granger D, Taylor Z, Continuous recording of blood oxygen tensions by polarography, J Appl Physiol 6(3) (1953) 189–93. [PubMed: 13096460]

[8]. Severinghaus JW, Astrup PB, History of blood gas analysis. IV. Leland Clark's oxygen electrode, J Clin Monit 2(2) (1986) 125–39. [PubMed: 3519875]

[9]. Severinghaus JW, The invention and development of blood gas analysis apparatus, Anesthesiology 97(1) (2002) 253–6. [PubMed: 12131126]

[10]. Xu Y, Zhang B, Messerli M, Randers-Pehrson G, Hei TK, Brenner DJ, Metabolic oxygen consumption measurement with a single-cell biosensor after particle microbeam irradiation, Radiat Environ Biophys 54(1) (2015) 137–144. [PubMed: 25335641]

[11]. Badwal SPS, Ciacchi FT & Haylock JW, Journal of Applied Electrochemistry, Springer, Berlin, 1988.

[12]. Chen R, Hahn CE, Farmery AD, A flowing liquid test system for assessing the linearity and time-response of rapid fibre optic oxygen partial pressure sensors, Respir Physiol Neurobiol 183(2) (2012) 100–7. [PubMed: 22688018]

[13]. O'Riordan TC, Zhdanov AV, Ponomarev GV, Papkovsky DB, Analysis of intracellular oxygen and metabolic responses of mammalian cells by time-resolved fluorometry, Anal Chem 79(24) (2007) 9414–9. [PubMed: 18001129]

[14]. Dmitriev RI, Papkovsky DB, Intracellular probes for imaging oxygen concentration: how good are they?, Methods Appl Fluoresc 3(3) (2015) 034001. [PubMed: 29148495]

[15]. Sharifi S, Behzadi S, Laurent S, Forrest ML, Stroeve P, Mahmoudi M, Toxicity of nanomaterials, Chem Soc Rev 41(6) (2012) 2323–43. [PubMed: 22170510]

[16]. Teeguarden JG, Hinderliter PM, Orr G, Thrall BD, Pounds JG, Particokinetics in vitro: dosimetry considerations for in vitro nanoparticle toxicity assessments, Toxicol Sci 95(2) (2007) 300–12. [PubMed: 17098817]

[17]. Bambot SB, Holavanahali R, Lakowicz JR, Carter GM, Rao G, Phase fluorometric sterilizable optical oxygen sensor, Biotechnol Bioeng 43(11) (1994) 1139–45. [PubMed: 18615527]

[18]. Gryczynski I, Gryczynski Z, Rao G, Lakowicz JR, Polarization-based oxygen sensor, Analyst 124(7) (1999) 1041–4. [PubMed: 10736861]

[19]. Acosta MA, Velasquez M, Williams K, Ross JM, Leach JB, Fluorescent silica particles for monitoring oxygen levels in three-dimensional heterogeneous cellular structures, Biotechnol Bioeng 109(10) (2012) 2663–70. [PubMed: 22511120]

[20]. Acosta MA, Ymele-Leki P, Kostov YV, Leach JB, Fluorescent microparticles for sensing cell microenvironment oxygen levels within 3D scaffolds, Biomaterials 30(17) (2009) 3068–74. [PubMed: 19285719]

[21]. Wang L, Acosta MA, Leach JB, Carrier RL, Spatially monitoring oxygen level in 3D microfabricated cell culture systems using optical oxygen sensing beads, Lab Chip 13(8) (2013) 1586–92. [PubMed: 23443975]

[22]. Rogers GW, Brand MD, Petrosyan S, Ashok D, Elorza AA, Ferrick DA, Murphy AN, High throughput microplate respiratory measurements using minimal quantities of isolated mitochondria, PLoS One 6(7) (2011) e21746. [PubMed: 21799747]

[23]. Boyman L, Hiller R, Lederer WJ, Khananshvili D, Direct Loading of the purified endogenous inhibitor into the cytoplasm of patched cardiomyocytes blocks the ion currents and calcium transport through the NCX1 protein, Biochemistry 47(25) (2008) 6602–11. [PubMed: 18507397]

[24]. Carraway ER, Demas JN, Degraff BA, Bacon JR, Photophysics and Photochemistry of Oxygen Sensors Based on Luminescent Transition-Metal Complexes, Anal Chem 63(4) (1991) 337–342.

[25]. Boyman L, Chikando AC, Williams GS, Khairallah RJ, Kettlewell S, Ward CW, Smith GL, Kao JP, Lederer WJ, Calcium movement in cardiac mitochondria, Biophys J 107(6) (2014) 1289–301. [PubMed: 25229137]

[26]. Murry CE, Jennings RB, Reimer KA, Preconditioning with ischemia: a delay of lethal cell injury in ischemic myocardium, Circulation 74(5) (1986) 1124–36. [PubMed: 3769170]

[27]. Jennings RB, Reimer KA, The cell biology of acute myocardial ischemia, Annual review of medicine 42 (1991) 225–46.

[28]. Halestrap AP, A pore way to die: the role of mitochondria in reperfusion injury and cardioprotection, Biochem Soc Trans 38(4) (2010) 841–60. [PubMed: 20658967]

[29]. Williams GS, Boyman L, Lederer WJ, Mitochondrial calcium and the regulation of metabolism in the heart, J Mol Cell Cardiol 78 (2015) 35–45. [PubMed: 25450609]

[30]. Karch J, Molkentin JD, Identifying the components of the elusive mitochondrial permeability transition pore, Proc Natl Acad Sci U S A 111(29) (2014) 10396–7. [PubMed: 25002521]

[31]. Szabo I, De Pinto V, Zoratti M, The mitochondrial permeability transition pore may comprise VDAC molecules. II. The electrophysiological properties of VdAc are compatible with those of the mitochondrial megachannel, FEBS Lett 330(2) (1993) 206–10. [PubMed: 7689984]

[32]. Giorgio V, von Stockum S, Antoniel M, Fabbro A, Fogolari F, Forte M, Glick GD, Petronilli V, Zoratti M, Szabo I, Lippe G, Bernardi P, Dimers of mitochondrial ATP synthase form the permeability transition pore, Proc Natl Acad Sci U S A 110(15) (2013) 5887–92. [PubMed: 23530243]

[33]. Halestrap AP, Davidson AM, Inhibition of Ca2(+)-induced large-amplitude swelling of liver and heart mitochondria by cyclosporin is probably caused by the inhibitor binding to mitochondrial-matrix peptidyl-prolyl cis-trans isomerase and preventing it interacting with the adenine nucleotide translocase, Biochem J 268(1) (1990) 153–60. [PubMed: 2160810]

[34]. Alavian KN, Beutner G, Lazrove E, Sacchetti S, Park HA, Licznerski P, Li H, Nabili P, Hockensmith K, Graham M, Porter GA Jr., Jonas EA, An uncoupling channel within the c-subunit ring of the F1FO ATP synthase is the mitochondrial permeability transition pore, Proc Natl Acad Sci U S A 111(29) (2014) 10580–5. [PubMed: 24979777]

[35]. Shanmughapriya S, Rajan S, Hoffman NE, Higgins AM, Tomar D, Nemani N, Hines KJ, Smith DJ, Eguchi A, Vallem S, Shaikh F, Cheung M, Leonard NJ, Stolakis RS, Wolfers MP, Ibetti J, Chuprun JK, Jog NR, Houser SR, Koch WJ, Elrod JW, Madesh M, SPG7 Is an Essential and Conserved Component of the Mitochondrial Permeability Transition Pore, Mol Cell 60(1) (2015) 47–62. [PubMed: 26387735]

[36]. Kokoszka JE, Waymire KG, Levy SE, Sligh JE, Cai J, Jones DP, MacGregor GR, Wallace DC, The ADP/ATP translocator is not essential for the mitochondrial permeability transition pore, Nature 427(6973) (2004) 461–5. [PubMed: 14749836]

[37]. Zhou W, Marinelli F, Nief C, Faraldo-Gomez JD, Atomistic simulations indicate the c-subunit ring of the F1Fo ATP synthase is not the mitochondrial permeability transition pore, Elife 6 (2017).

[38]. Halestrap AP, The C Ring of the F1Fo ATP Synthase Forms the Mitochondrial Permeability Transition Pore: A Critical Appraisal, Front Oncol 4 (2014) 234. [PubMed: 25202683]

[39]. He J, Ford HC, Carroll J, Ding S, Fearnley IM, Walker JE, Persistence of the mitochondrial permeability transition in the absence of subunit c of human ATP synthase, Proc Natl Acad Sci U S A 114(13) (2017) 3409–3414. [PubMed: 28289229]

[40]. Marquis BJ, Love SA, Braun KL, Haynes CL, Analytical methods to assess nanoparticle toxicity, Analyst 134(3) (2009) 425–39. [PubMed: 19238274]

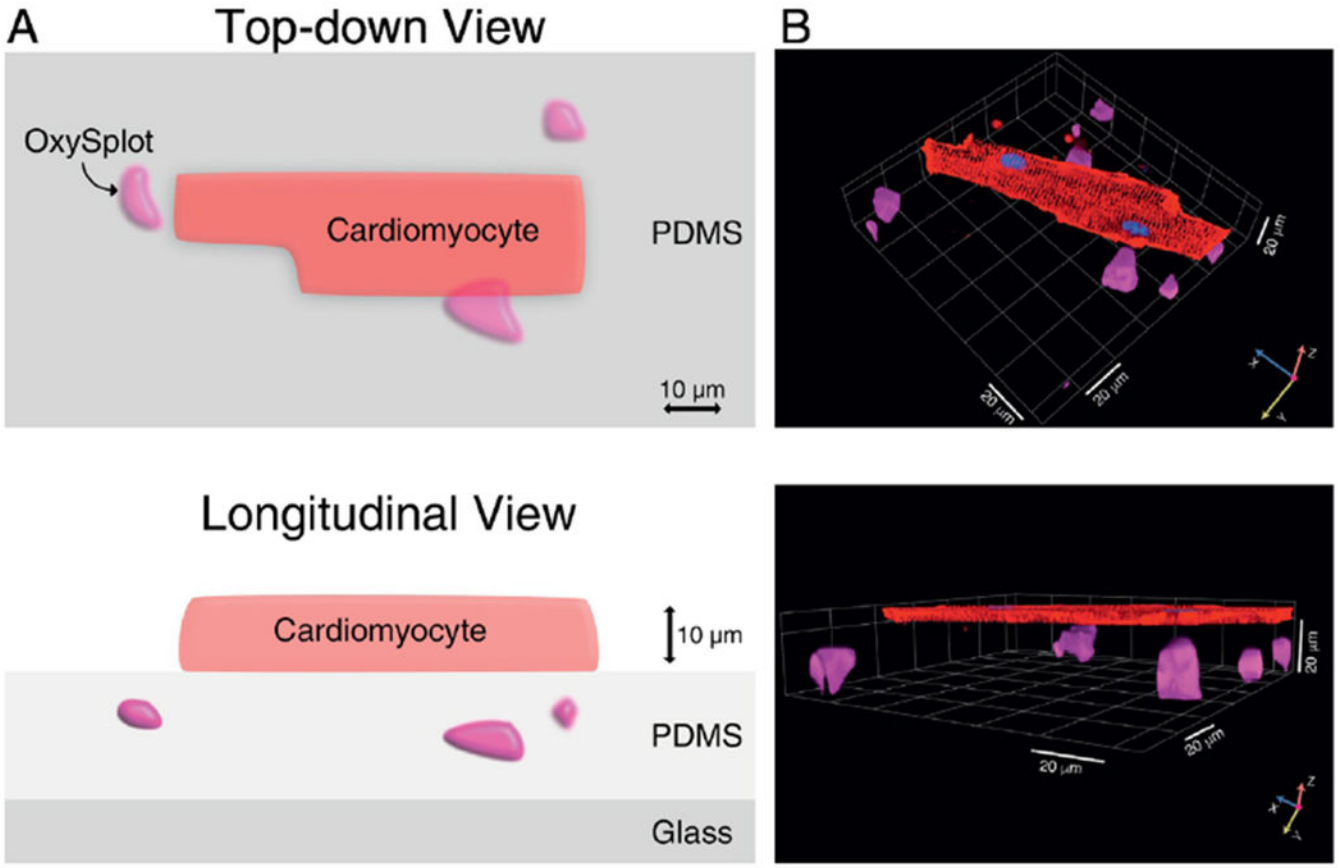

Figure 1. Simultaneous measurement of local pO_2 and high resolution cellular imaging.

A, Diagrammatic illustration of the method showing a single, isolated cardiomyocyte in close proximity to the OxySplot particles. **B,** High-resolution 3D reconstruction of confocal Z-stack images of a cardiomyocyte stained with di-8-ANEPPS to label the sarcolemmal membrane (red), Hoechst-33342 to label nuclear DNA (blue), and OxySplots (purple).

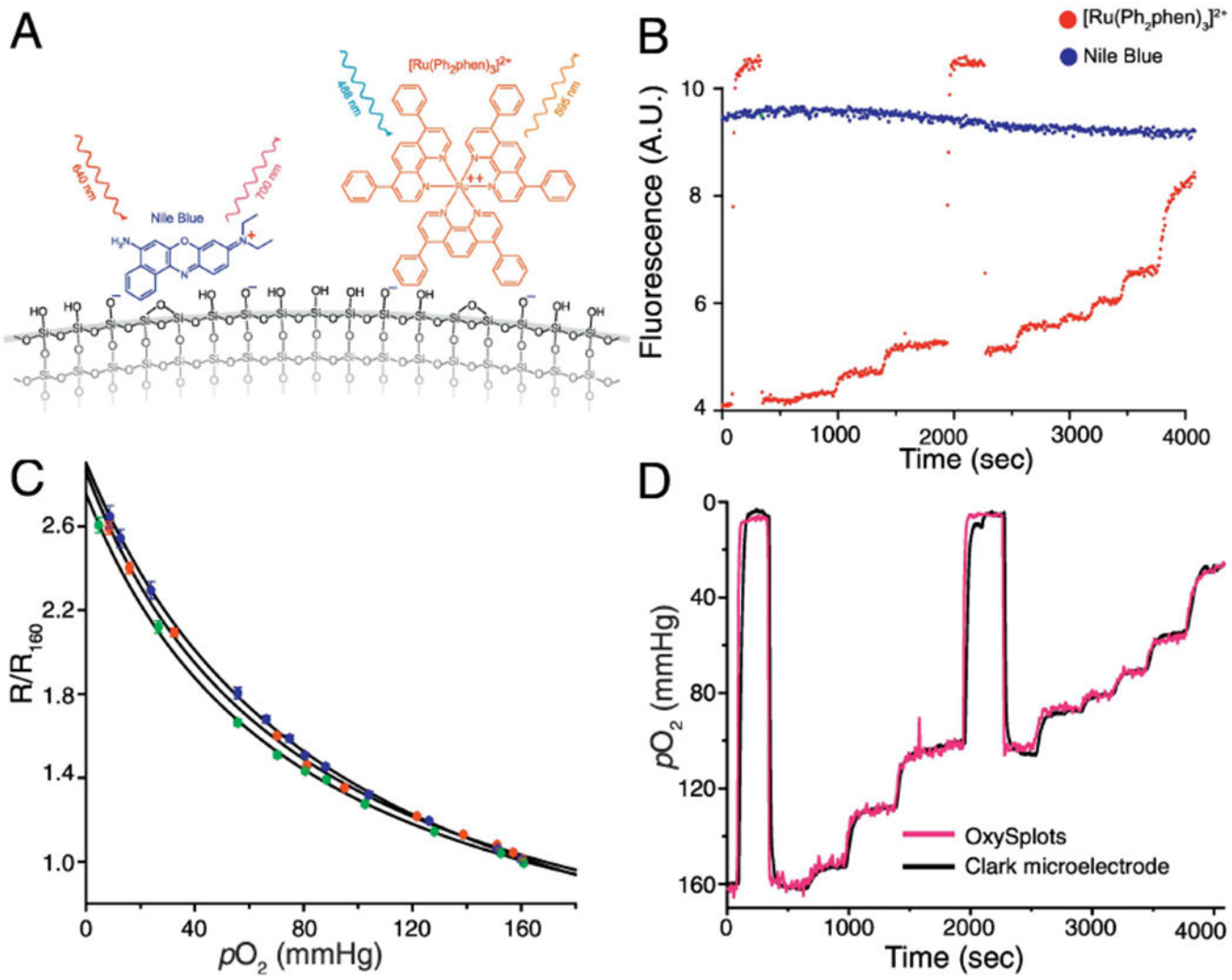

Figure 2. Formulation and Calibration of OxySplots.

A, Schematic showing OxySplot fluorophores ($[Ru(Ph_2phen)_3]^{2+}$ and Nile blue) adsorbed to silica gel. **B,** Representative traces showing florescence of both OxySplot fluorophores over time for calibration shown in Fig. 2C. **C,** Normalized, steady-state fluorescence measurements (each color indicates repeated calibration) from OxySplot (R/R_{160}) versus instantaneous pO_2 measurements via a Clark-type O_2 microelectrode. Fit lines are two-site Stern–Volmer model (n=3 pO_2 calibrations). **D,** Simultaneous, calibrated measurements of pO_2 via OxySplot and Clark-type oxygen microelectrode (see SD for more details).

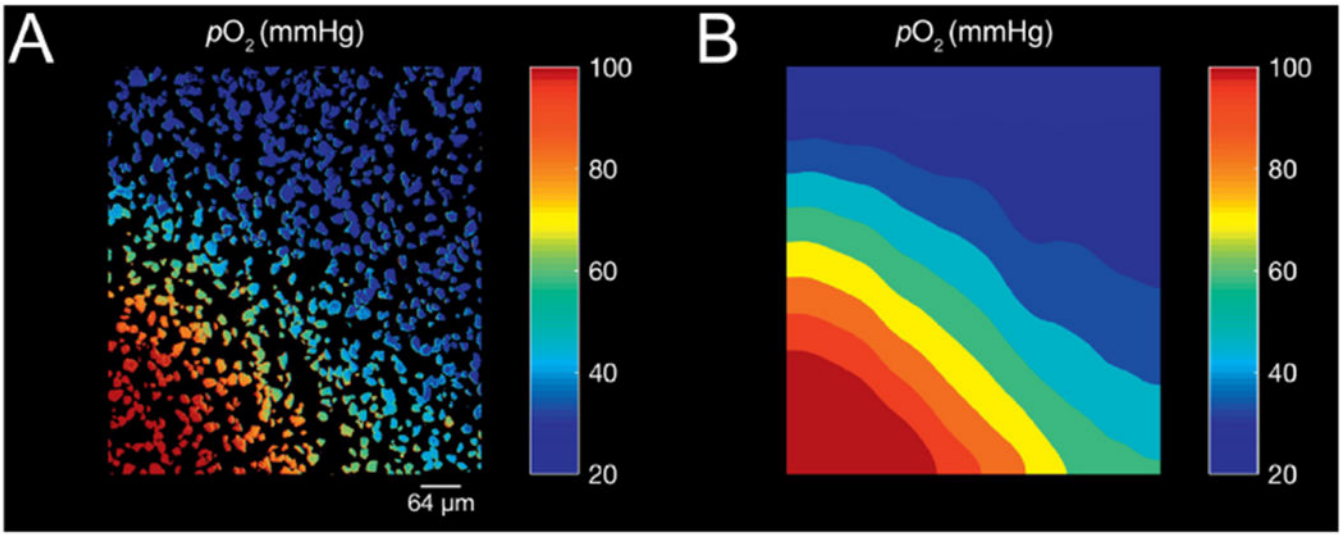

Figure 3. Local Gradients of pO_2.

A, Calibrated pO_2 as reported by a dense layer of OxySplots **B,** Interpolated heat-map of pO_2 gradient. Bulk, bath perfusion using O_2 depleted solution with micro-perfusion manifold emitting O_2 rich solution positioned in the bottom left of field of view.

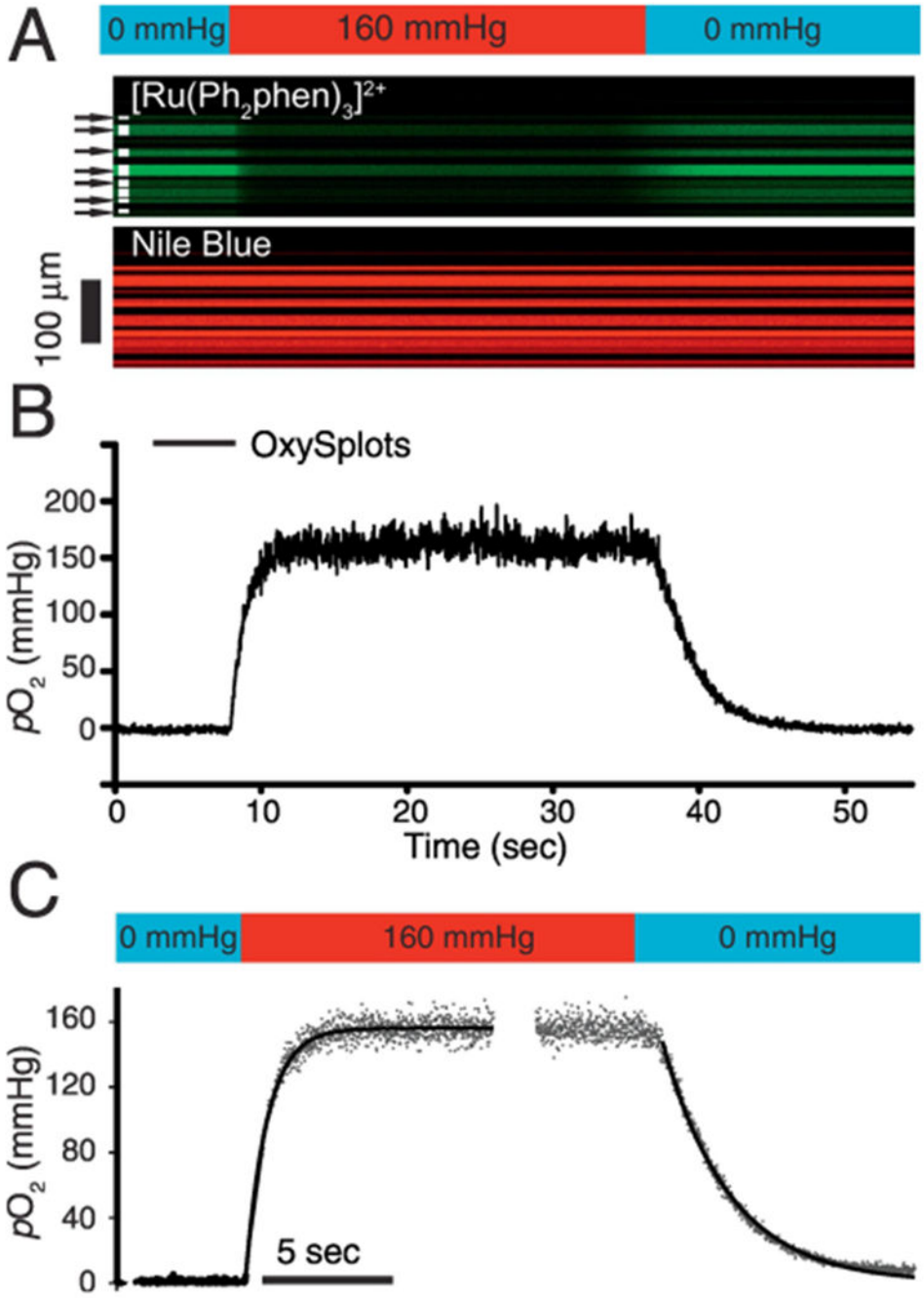

Figure 4. Measuring rapid changes of pO_2 with OxySplots.

A, confocal line-scan image showing the time-dependent fluorescence of $[Ru(Ph_2phen)_3]^{2+}$ and Nile blue. Confocal measurements are done during abrupt local (bathing) solution switch from anoxic solution to hyperoxic (160 mmHg), and back again to anoxic solution (for more details see Fig. S2). **B,** pO_2 measurements via OxySplots (black line, 8 silica particles indicated in **A**). **C,** Double exponential fits to the pO_2 rise ($t_{0.5}$ =0.7 sec, n=6 experiments) and pO_2 decay ($t_{0.5}$ =1.63 sec, n=6 experiments).

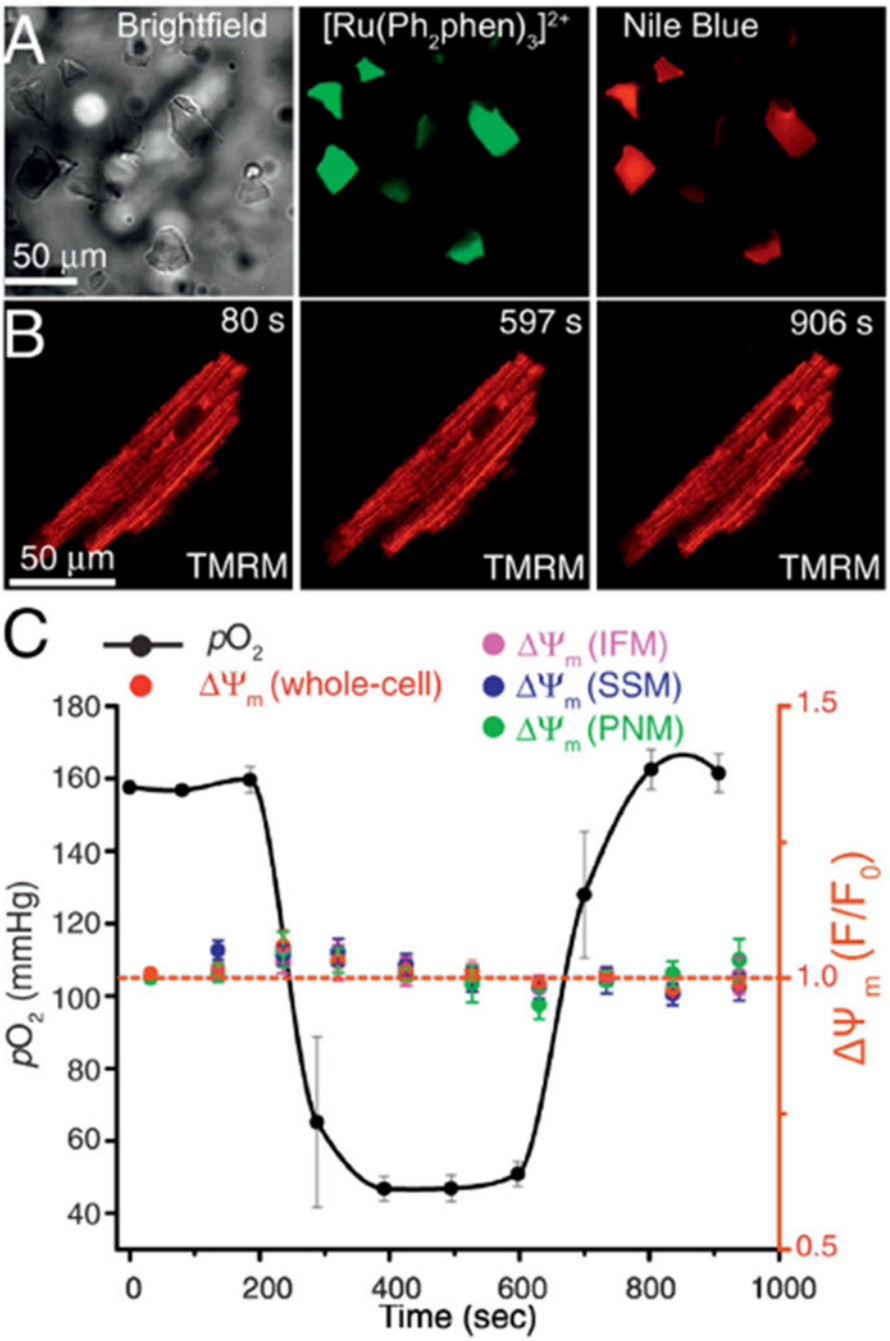

Figure 5. Mitochondrial inner membrane potential in single cardiac cells during changes of pericellular pO_2.

A, Left, bright-field image (112×112 μm) showing OxySplots. Also visible is the shadow of a cardiomyocyte adherent to the top of the PDMS layer 36 μm above the shown imaging plane. Middle, confocal image showing the fluorescence of $[Ru(Ph_2phen)_3]^{2+}$. Right, confocal image showing the fluorescence of Nile blue. **B,** Confocal images of a TMRM loaded cardiomyocyte captured at the indicated time points during the experiments shown in panel C. **C,** The time course of changes in pO_2 (black) and of TMRM fluorescent signals

from the whole-cell (red), from intermyofibrillar mitochondria (IFM), from subsarcolemmal mitochondria (SSM), and from perinuclear mitochondria (PNM).

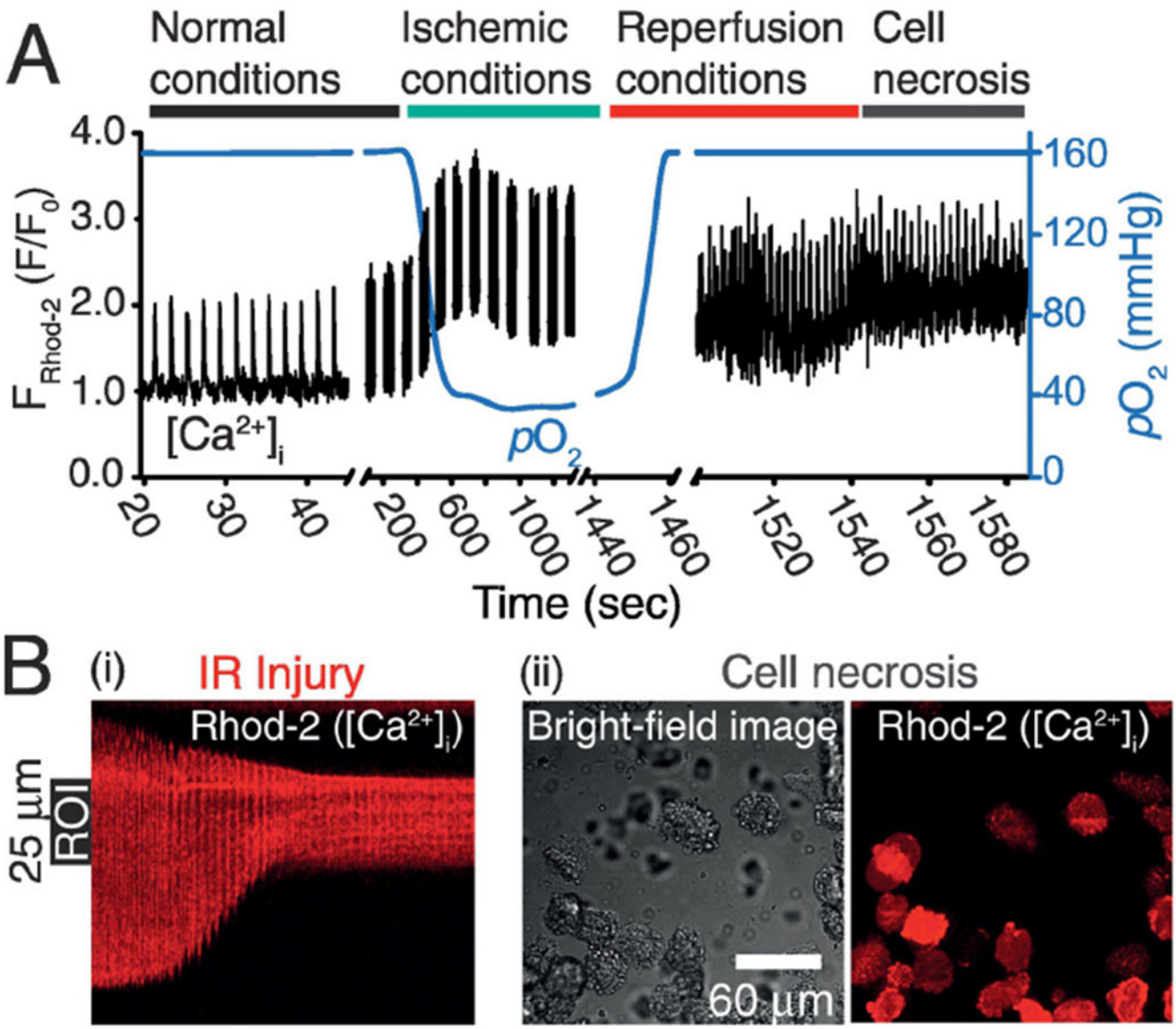

Figure 6. Isolated ventricular cardiomyocytes as an ischemia-reperfusion injury model.

A, the time course of changes in pO_2 (blue line) and Rhod-2 fluorescence (black line). The Ca^{2+}-sensitive fluorophore Rhod-2 is used for $[Ca^{2+}]_i$ measurements. Fluorescence line-scan measurements of $[Ca^{2+}]_i$ are acquired along the longitudinal axis of a cardiomyocyte. During each imaging break the automated focal plane adjustment function of the microscope switches back and forth between two planes; 1) the imaging plane of the cardiomyocyte and 2) that of the OxySplots for pO_2 measurements. The cell is initially perfused with Normal Tyrode, and then with ischemic Tyrode buffer, followed by Normal Tyrode again, as indicated. **B,** (i) the line-scan image acquired during the reperfusion stage, (ii) 225 µm × 225 µm bright field and confocal image of the cells captured 10 seconds after the line-scan imaging in (i) ended. During the entire time course of the experiment 0.5 Hz electrical field stimulation is applied.